REPORT No. 842

SOME EFFECTS OF COMPRESSIBILITY ON THE FLOW THROUGH FANS AND TURBINES

By W. Perl and H. T. Epstein

SUMMARY

The laws of conservation of mass, momentum, and energy are applied to the compressible flow through a two-dimensional cascade of airfoils. A fundamental relation between the ultimate upstream and downstream flow angles, the inlet Mach number, and the pressure ratio across the cascade is derived. Comparison with the corresponding relation for incompressible flow shows large differences.

The fundamental relation reveals two ranges of flow angles and inlet Mach numbers, for which no ideal pressure ratio exists. One of these nonideal operating ranges is analogous to a similar type in incompressible flow. The other is characteristic only of compressible flow.

The effect of variable axial-flow area is treated. Some implications of the basic conservation laws in the case of nonideal flow through cascades are discussed.

INTRODUCTION

In the endeavor to obtain high pressure rise from axial-flow compressors, the operating speeds have been increased in recent years to compressibility speeds. The precise extent of validity at these speeds of the incompressible-flow methods of design of axial-flow compressor blading appears not to have been considered heretofore.

In this paper, which describes results of a theoretical investigation made at the NACA Cleveland laboratory during 1944 and 1945, the extent of validity is determined in the isentropic case by applying the compressible-flow laws to the ultimate upstream and downstream flow conditions in a two-dimensional cascade of airfoils. The resulting equations relating the pressure ratio across the cascade, the flow angles, and the inlet Mach number are compared with the corresponding incompressible-flow relations.

The results apply to both fan-type and turbine-type cascades. Although compressible-flow relations are generally used in the design of turbine cascades and, less generally, in the design of fan cascades, it is thought that the compact form of the results presented herein will render them more easily applicable than the other methods now in use.

SYMBOLS

The following symbols are used in this report:

A	flow area perpendicular to axial direction
c_p	specific heat at constant pressure
M	Mach number of flow
p	static pressure
R	gas constant
S	entropy
s	cascade spacing
t	temperature
u	velocity in x-direction
v	velocity in y-direction
w	resultant velocity; also mean velocity
X	x-direction (tangential) force per blade per unit span
Y	y-direction (normal) force per blade per unit span
γ	ratio of specific heats
λ	angle of flow measured from axial direction
ρ	density

Subscripts:

1	upstream of cascade
2	downstream of cascade
s	stagnation

VELOCITY-DIAGRAM RELATIONS FOR COMPRESSIBLE CASCADE FLOW

GOVERNING EQUATIONS

Consider the ultimate upstream and downstream compressible-flow conditions, or the velocity diagram, for the cascade of airfoils representing a fan or a turbine-blade arrangement (fig. 1). The conservation laws applied between the up-

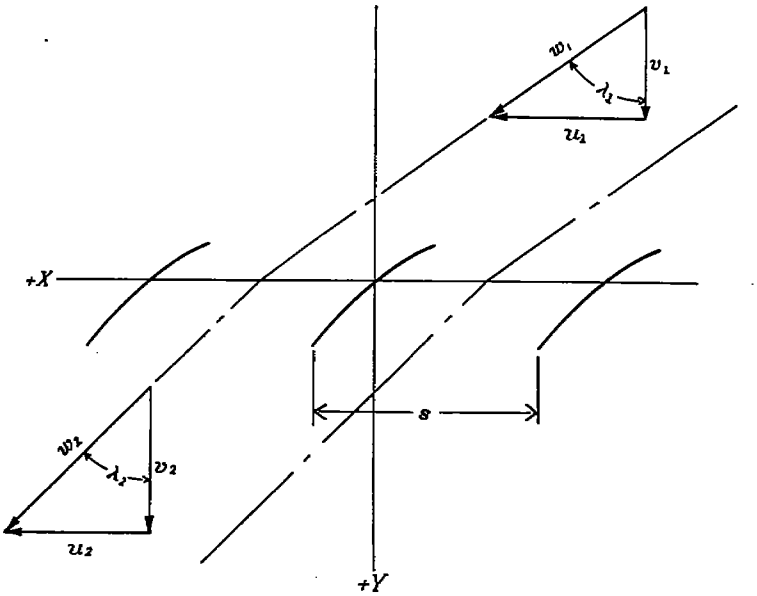

FIGURE 1.—Two-dimensional cascade.

842951—50——10

stream section and the downstream section where the flow is assumed to be uniform and to pass through equal areas are:

Continuity

$$\rho_1 v_1 = \rho_2 v_2 \tag{1}$$

Energy

$$c_p t_1 + \frac{1}{2} w_1^2 = c_p t_2 + \frac{1}{2} w_2^2 \tag{2}$$

Momentum

$$\text{Normal, } y\text{-direction: } \frac{Y}{s} = p_1 - p_2 + \rho_1 v_1^2 - \rho_2 v_2^2 \tag{3}$$

$$\text{Tangential, } x\text{-direction: } \frac{X}{s} = \rho_1 v_1 (u_1 - u_2) \tag{4}$$

In addition, there is the gas law

$$p = \rho R t \tag{5}$$

and the isentropic relation

$$\frac{p_2}{p_1} = \left(\frac{\rho_2}{\rho_1}\right)^{\gamma} \tag{6}$$

(The assumption of the isentropic exponent γ prevents the direct application of the results to fan or turbine blading. It appears, however, that use of a suitable polytropic exponent $n \neq \gamma$ allows direct application in many cases.)

Substitution of equations (1), (5), and (6) in equation (2) yields the fundamental relation between the flow angles λ_1 and λ_2, the pressure ratio p_2/p_1, and the inlet Mach number M_1:

$$\frac{\cos \lambda_1}{\cos \lambda_2} = \left(\frac{p_2}{p_1}\right)^{\frac{1}{\gamma}} \sqrt{1 - \frac{2}{(\gamma - 1) M_1^2} \left[\left(\frac{p_2}{p_1}\right)^{\frac{\gamma - 1}{\gamma}} - 1 \right]} \tag{7}$$

For the case of incompressible flow, the expression corresponding to equation (7) may be derived from the equations corresponding to (1) and (2); namely

$$\text{Continuity (incompressible): } v_1 = v_2 \tag{8}$$

$$\text{Bernoulli (incompressible): } p_1 + \frac{1}{2} \rho_1 w_1^2 = p_2 + \frac{1}{2} \rho_1 w_2^2 \tag{9}$$

The result is

$$\frac{\cos \lambda_1}{\cos \lambda_2} = \sqrt{1 - \frac{2}{\gamma M_1^2} \left(\frac{p_2}{p_1} - 1\right)} \tag{10}$$

in which the substitution

$$M_1^2 = \frac{w_1^2}{\gamma \frac{p_1}{\rho_2}} \tag{11}$$

has been made for comparison with the compressible-flow relation (equation (7)). Equation (10) may also be derived as the limiting form of equation (7) when the specific-heat ratio γ approaches infinity. (The incompressible fluid may be regarded as the limiting form of a compressible perfect fluid in which the velocity of sound $\sqrt{\gamma \frac{p}{\rho}}$ approaches infinity. Inasmuch as p and ρ remain finite, γ must become infinite.)

GRAPHICAL REPRESENTATION OF EQUATIONS

For a given inlet Mach number M_1 and pressure ratio p_2/p_1, equation (7) shows that the flow angles λ_1 and λ_2 are not specified but only their cosine ratio. A plot of the cosine ratio $\cos \lambda_1 / \cos \lambda_2$ against the flow deflection $\lambda_1 - \lambda_2$, with λ_1 or λ_2 as a parameter (fig. 2), illustrates the possible individual flow angles and deflections for a given cosine ratio.

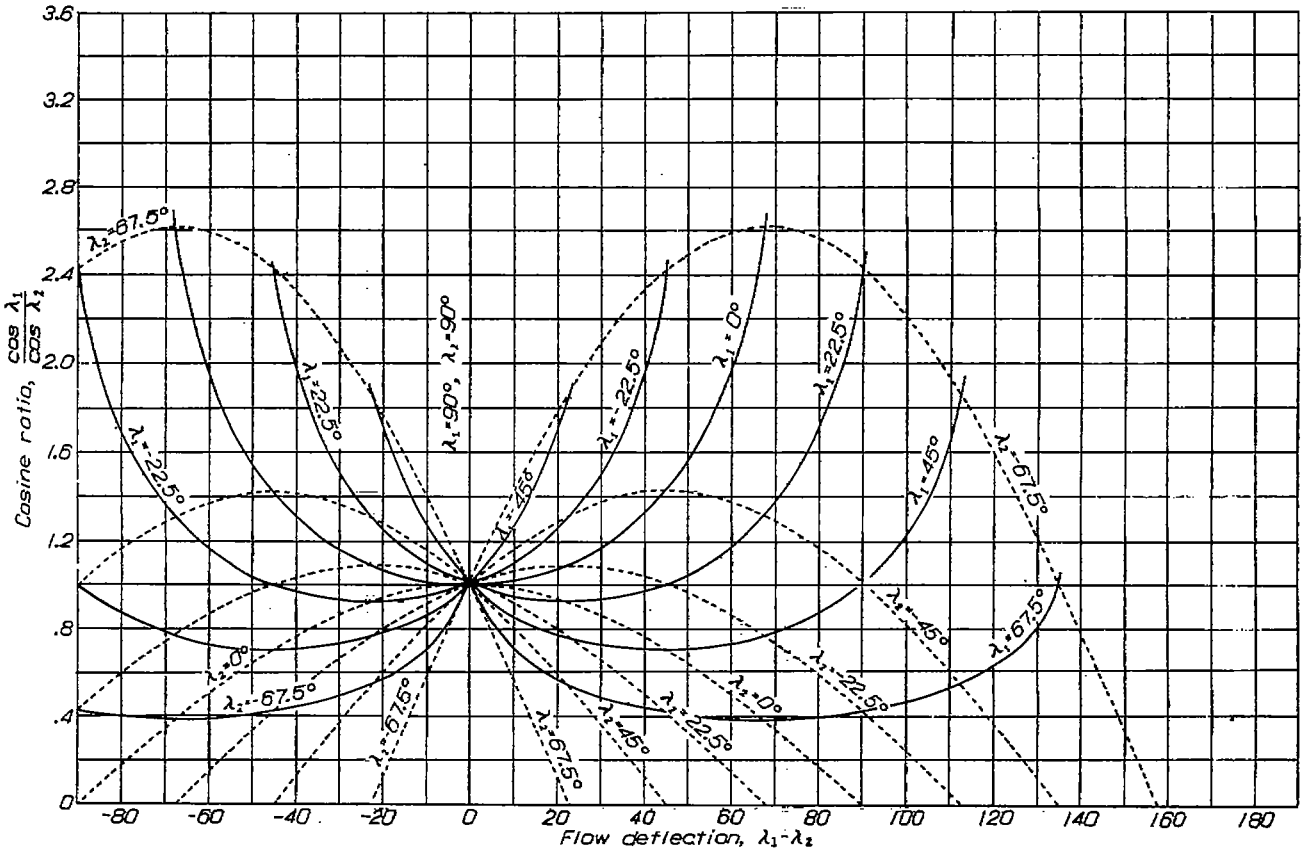

FIGURE 2.—Relation of $\frac{\cos \lambda_1}{\cos \lambda_2}$ to turning angle of flow.

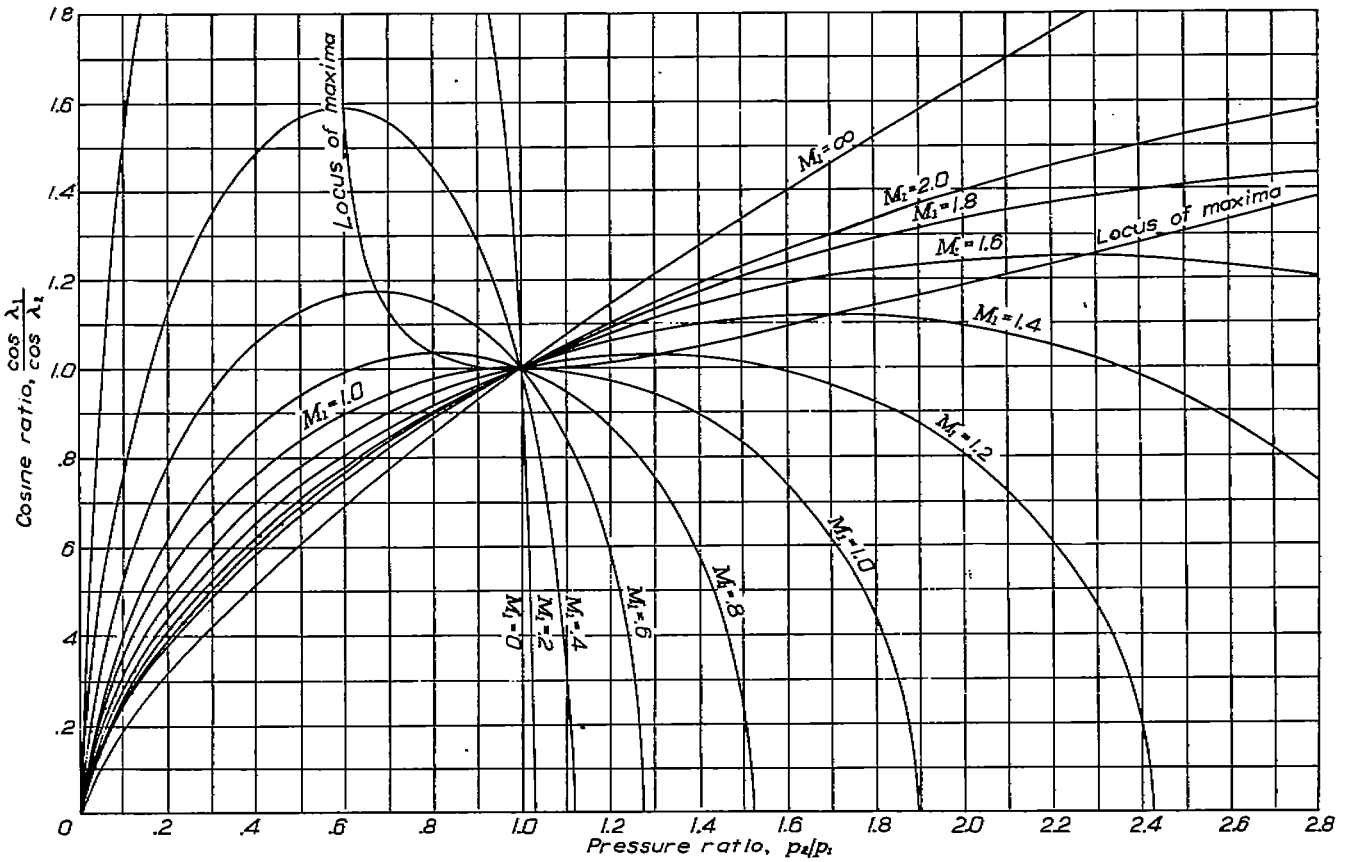

FIGURE 3.—Relation of compressible flow angles to p_2/p_1 for various inlet Mach numbers.

The flow angles λ_1 and λ_2 may be visualized as the stagger angles of the tangents to the camber line of the cascade blading at the leading edge and the trailing edge, respectively. For low-speed flow, at least, and for shock-free entry, this correspondence is approximately valid for cascade solidities of the order of unity (solidity=blade chord/blade spacing) and increases in validity with the solidity.

The contours representing equation (7) are shown in figures 3 and 4. Several of the contours of figures 3 and 4 are compared with the corresponding contours in the incompressible case (equation (10)) in figures 4 and 5.

COMPARISON OF COMPRESSIBLE AND INCOMPRESSIBLE EQUATIONS

The comparison between the compressible and incompressible equations (figs. 4 and 5) reveals considerable differences except in the pressure-rise range $(p_2/p_1)>1$ at low inlet Mach number ($M_1<0.4$). Outside this range consider, for example, the determination of the blade camber of a high-solidity pressure-rise cascade designed to operate at an inlet-flow angle of 45°, an inlet Mach number of 0.80, and a pressure ratio of 1.2. (Camber is defined as the difference in angle between leading-edge and trailing-edge camber-line tangents. Camber therefore approximates $\lambda_1-\lambda_2$ for high-solidity cascades.) By the incompressible contour $M_1=0.8$ in figure 5 and by use of figure 2, the camber should be 26.9°. According to the compressible curve, on the other hand, the camber should be 9.4°, or 65 percent smaller. If the inlet Mach number is increased to unity, the results are:

Incompressible camber, degrees	11.8
Compressible camber, degrees	1.5

As an example of the differences between compressible and incompressible flow in the case of a pressure drop through the cascade, assume $\lambda_1=0°$, $M_1=0.80$, and $p_2/p_1=0.7$. Then from figures 2 and 5

Incompressible-flow deflection, degrees	39.3
Compressible-flow deflection, degrees	13.1

Thus, the effect of compressibility in the normal operating range of moderate pressure ratios is to lower substantially the required flow deflection for a given pressure ratio.

On the other hand, for given flow angles, that is, given $\cos \lambda_1/\cos \lambda_2$, figure 4 shows that for normal compressor operation, $(\cos \lambda_1/\cos \lambda_2)<1$ and $(p_2/p_1)>1$, the compressible pressure ratio increases with the inlet Mach number M_1 at a greater rate than the incompressible pressure ratio. For example, if $\cos \lambda_1/\cos \lambda_2=0.8$ in normal compressor operation and $M_1=0.8$, the incompressible pressure ratio is 1.16 and the compressible pressure ratio is 1.27.

FURTHER DISCUSSION OF THE COMPRESSIBLE CASE

The surface representing the fundamental equation (7) is the locus of all possible isentropic (loss-free) operating conditions of the cascade and no others. The contour projections of this surface show that certain ranges of operating conditions are unattainable in isentropic flow; thus, in figure 5, there is no inlet Mach number M_1 to correspond to cosine ratios $\cos \lambda_1/\cos \lambda_2$ and pressure ratios p_2/p_1 in the plane regions AOB and COD.

The reason for such nonideal regions can be seen by analogy with the incompressible case. The incompressible M_1 contours entirely exclude the first and the third quadrants, relative to point O as origin. Consider the case

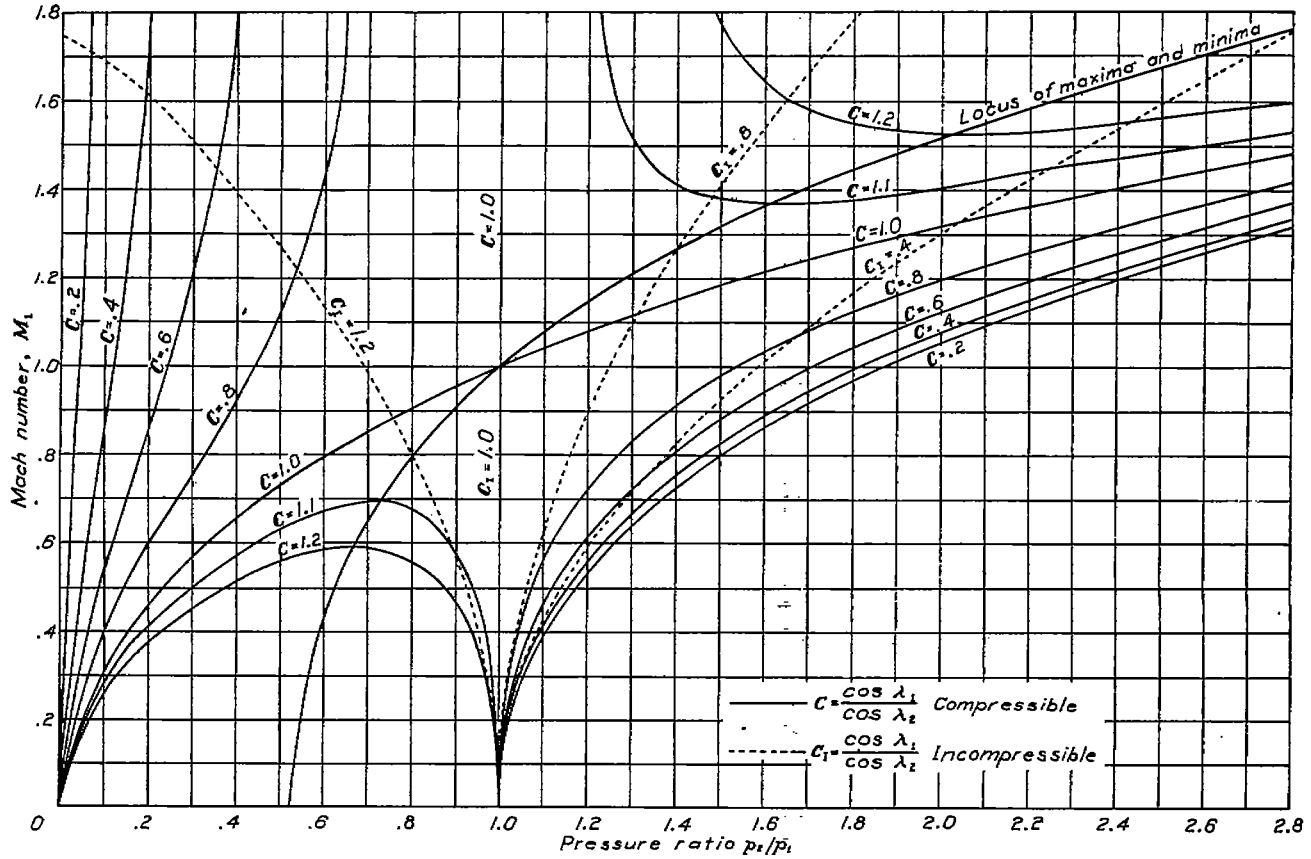

FIGURE 4.—Relation of compressible and incompressible inlet Mach numbers to p_2/p_1 for various flow angles.

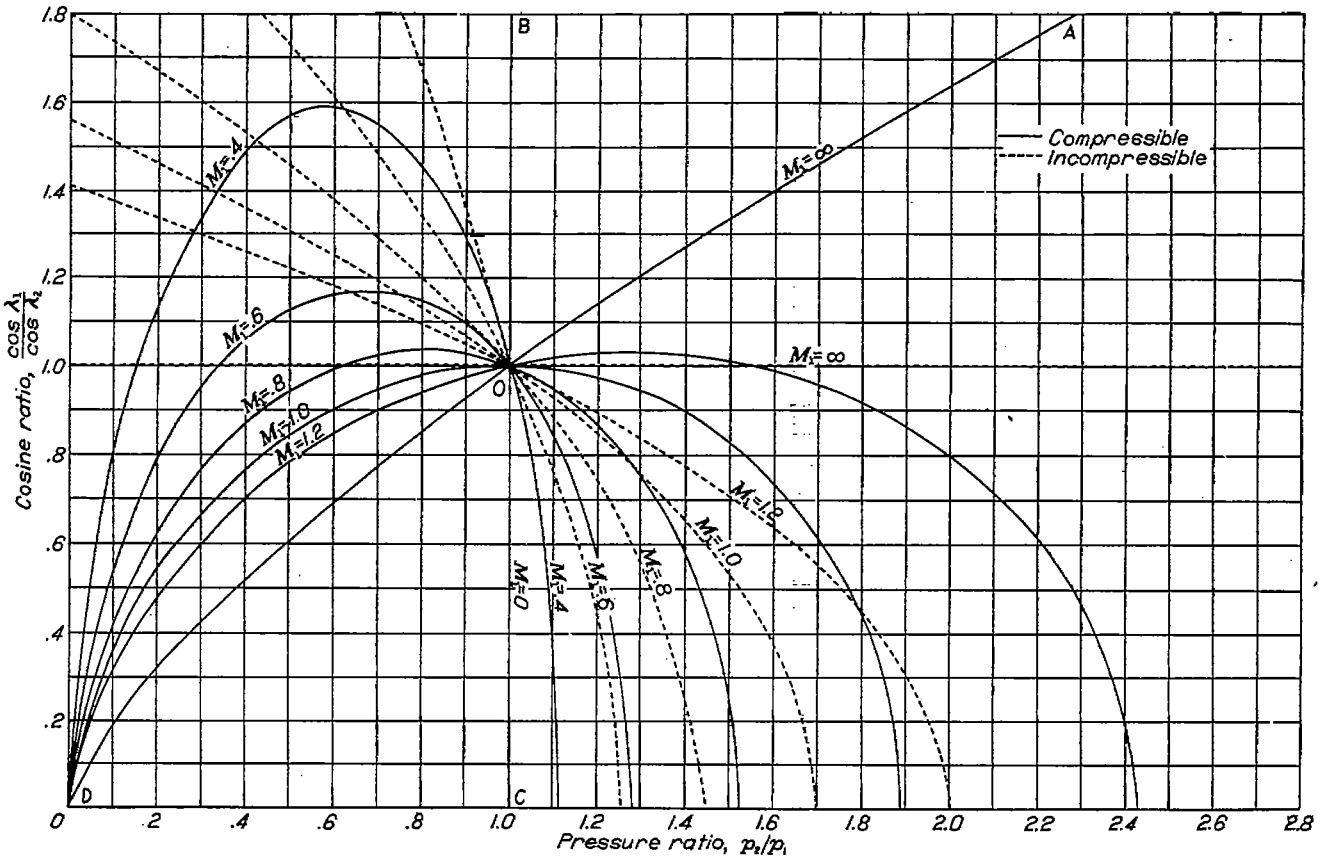

FIGURE 5.—Comparison of compressible and incompressible flow angles as function of p_2/p_1 for various inlet Mach numbers.

$(\cos\lambda_1/\cos\lambda_2)>1$. Inasmuch as the exit angle λ_2 is greater than the entrance angle λ_1, the exit tangential-velocity component is greater than the entrance tangential-velocity component. Because the axial velocity is constant, a pressure drop $(p_2/p_1)<1$ is required in accordance with Bernoulli's theorem, and the operation point for $(\cos\lambda_1/\cos\lambda_2)>1$ cannot lie in the first quadrant but must lie in the second quadrant. Similarly, operating points for $(\cos\lambda_1/\cos\lambda_2)>1$ must lie in the fourth quadrant. The partial overlapping of the compressible-flow curves into the first and third quadrants is due to the influence of compressibility on the axial component of velocity.

Another type of nonideal region is shown in figure 4. For fixed $(\cos\lambda_1/\cos\lambda_2)>1$, an isentropically impossible range of inlet Mach numbers exists, which increases with $\cos\lambda_1/\cos\lambda_2$. At $\cos\lambda_1/\cos\lambda_2=1.1$, for example, the excluded M_1 range is $0.695<M_1<1.37$. This type of nonideal range is not present in the incompressible case shown as the dashed curves of figure 4. The lower limiting inlet Mach numbers of this range correspond to maximum flow through the cascade, for, because $\cos\lambda_1/\cos\lambda_2$ is constant along each curve in figure 4, the maxima of M_1 also correspond to the maxima of M_1 $(\cos\lambda_1/\cos\lambda_2)$. For a given high-solidity cascade, λ_2 varies only slightly as the inlet conditions are varied; therefore, $M_1\cos\lambda_1$, which is proportional to the flow through the cascade, is likewise a maximum at these points. This particular limiting Mach number is independent of the blade-shape details and, hence, of the ratio of minimum flow area to inlet area.

If a cascade is designed to operate in an isentropically impossible region, presumably much greater losses, caused by flow separation and shock waves, will occur than would be encountered at an ideally permissible operating point. Such nonideal designs appear to be not at all unusual on the basis of incompressible-flow theory.

Of considerable interest is the fact that, at the maxima and the minima of all $\cos\lambda_1/\cos\lambda_2$ contours, the exit Mach number M_2 is unity, which may be shown as follows: The maxima and the minima of the $\cos\lambda_1/\cos\lambda_2$ contours in figure 4 correspond to the maxima of the M_1 contours in figure 3. The loci of these maxima are indicated in both figures. The condition for maximum $\cos\lambda_1/\cos\lambda_2$ along an M_1 contour is obtained by differentiation of equation (7) as

$$M_1\frac{\cos\lambda_1}{\cos\lambda_2}=\left(\frac{p_2}{p_1}\right)^{\frac{\gamma+1}{2\gamma}} \tag{12}$$

The downstream Mach number M_2

$$M_2=\frac{w_2^2}{\gamma\frac{p_2}{\rho_2}} \tag{13}$$

can now be written, with the aid of equations (1), (2), (5), and (6), as

$$M_2=\frac{M_1\frac{\cos\lambda_1}{\cos\lambda_2}}{\left(\frac{p_2}{p_1}\right)^{\frac{\gamma+1}{2\gamma}}} \tag{14}$$

Substitution of equation (12) in equation (14) yields the desired result, namely, $M_2=1$. In the limiting case $M_1=0$, equations (12) and (7) show that

$$\left(\frac{\cos\lambda_1}{\cos\lambda_2}\right)_{M_1=0}=\infty$$

$$\left(\frac{p_2}{p_1}\right)_{M_1=0}=\left(\frac{2}{\gamma+1}\right)^{\frac{\gamma}{\gamma-1}}=0.528 \qquad (\gamma=1.4)$$

This limiting pressure ratio is the same as the critical pressure ratio for local Mach number of unity in one-dimensional compressible flow.

Points to the right of the maximum on an M_1 contour (fig. 3) correspond to subsonic exit conditions $M_2<1$; whereas points to the left of the maximum correspond to supersonic exit conditions $M_2>1$. In figure 4 the subsonic exit region is to the right of the locus of maxima and minima and the supersonic exit region to the left. The proof is as follows: From general principles, the ideal continuous flow through a cascade is reversible; that is, equation (7) remains valid if the subscripts 1 and 2 are interchanged. This validity may also be shown directly by substitution of equation (14) in equation (7) to eliminate M_1. Consequently, the exit Mach number M_2 can be determined from the curves that represent equation (7); thus, in figure 3, the exit Mach number M_2 for the operating conditions M_1, p_2/p_1, and $\cos\lambda_1/\cos\lambda_2$ is obtained by interpolation from the M contours at the point for which the coordinates are the reciprocal quantities p_1/p_2 and $\cos\lambda_2/\cos\lambda_1$. This reciprocal relation, applied to the loci of the maximum points on the M_1 contours (fig. 3), yields the $M_1=1$ contour (where now $M_1=M_2$), by the proof previously given; therefore, the reciprocal relation applied to a point to the right of a maximum yields a point in the subsonic region relative to the $M_1=1$ contour and vice versa.

VARIABLE AXIAL-FLOW AREA

In many multistage compressors and turbines, the axial-flow area is continuously varied in order to maintain the axial-flow velocity constant. The effect of a change in axial-flow area through a cascade can be very simply taken into account in the preceding analysis. The equation of continuity (equation (1)) is now

$$\rho_1 v_1 A_1=\rho_2 v_2 A_2 \tag{15}$$

or

$$\rho_1 v_1 a=\rho_2 v_2 \tag{16}$$

where A_1 and A_2 are the axial-flow areas upstream and downstream, respectively, of the cascade, and

$$a\equiv\frac{A_1}{A_2} \tag{17}$$

The only change required in the fundamental equation (7) is that the flow-angle parameter $\cos\lambda_1/\cos\lambda_2$ be replaced by $a(\cos\lambda_1/\cos\lambda_2)$.

ENERGY RELATIONS FOR CASCADES

If the isentropic relation (equation (6)) is dropped, equations (1) to (5) relate ultimate conditions on each side of a cascade within which losses may occur. The equations may also be regarded as relating conditions across two sides of a line of discontinuity separating two regions of uniform flow, with the force densities X/s, Y/s acting on the fluid along the discontinuity. The oblique shock wave in supersonic flow represents the special case in which $X/s=Y/s=0$.

Without the isentropic relation there is, of course, no longer a unique dependence of the flow-angle ratio $\cos\lambda_1/\cos\lambda_2$ on the pressure ratio p_2/p_1 and the inlet Mach number M_1. (See equation (7).) Equations (1) to (5), however, yield information concerning the relation between the pressure ratios that might actually occur, the forces on the blade, and the losses in the cascade. Suppose, for example, that a high-solidity compressor cascade were designed for a certain ideal operating point. The ideal forces on the blades could be calculated from equations (3) and (4). In the actual flow the pressure ratio would be less than the ideal value. The flow angles, however, because of the high solidity, could be expected to remain nearly unaltered. On the assumption of an ideal flow-angle ratio and a smaller than ideal pressure ratio, the actual blade forces could be computed by equations (3) and (4). The vector difference between the actual resultant force and the ideal resultant force is a difference force caused by friction and shock-wave losses. The corresponding stagnation-pressure loss or, equivalently, the entropy increase across the cascade, can also be calculated.

An example of the type of computation just outlined follows: Among other things, it will be shown that the difference force is neither at right angles to the ideal resultant force nor in the direction of the mean relative flow. Although, as will be shown, the incompressible equations predict that the difference force is always in the axial direction, the compressible equations show that this is far from being the case.

The losses in cascade flow between an ultimate upstream and an ultimate downstream uniform-flow condition may be expressed in terms of the actual static-pressure ratio p_2/p_1 and the density ratio ρ_2/ρ_1 as follows: In the downstream condition, the ratio of stagnation pressure $p_{s,2}$ to static pressure p_2 is isentropically related to the corresponding temperature ratio as

$$\left(\frac{p_{s,2}}{p_2}\right)^{\frac{\gamma-1}{\gamma}}=\frac{t_{s,2}}{t_2}$$

Similarly, in the upstream condition,

$$\left(\frac{p_{s,1}}{p_1}\right)^{\frac{\gamma-1}{\gamma}}=\frac{t_{s,1}}{t_1}$$

If the preceding two equations are divided, remembering that $t_{s,1}=t_{s,2}$ because no energy is supplied from the outside, and if pressure and density are substituted for temperature by the gas law, there results

$$\frac{p_{s,2}}{p_{s,1}}=\frac{\left(\frac{\rho_2}{\rho_1}\right)^{\frac{\gamma}{\gamma-1}}}{\left(\frac{p_2}{p_1}\right)^{\frac{1}{\gamma-1}}} \tag{18}$$

In isentropic flow, equation (18) reduces, of course, to $p_{s,2}=p_{s,1}$. In an actual flow $p_{s,2}$ is less than $p_{s,1}$ corresponding to an entropy increase S_2-S_1, given by the well-known formula

$$S_2-S_1=R\log_e\frac{p_{s,1}}{p_{s,2}} \tag{19}$$

Substituting the normal velocity ratio v_2/v_1 into equation (18) yields, by the continuity equation (1),

$$\frac{p_{s,2}}{p_{s,1}}=\frac{1}{\left(\frac{v_2}{v_1}\right)^{\frac{\gamma}{\gamma-1}}\left(\frac{p_2}{p_1}\right)^{\frac{1}{\gamma-1}}} \tag{20}$$

The normal velocity ratio v_2/v_1 can be expressed in terms of the static-pressure ratio p_2/p_1, the inlet Mach number M_1, and the cosine ratio $\cos\lambda_1/\cos\lambda_2$ by equations (1), (2), and (5). The result is

$$\frac{v_2}{v_1}=\frac{1}{(\gamma-1)M_1^2\frac{\cos^2\lambda_1}{\cos^2\lambda_2}}\frac{p_2}{p_1}\left[\sqrt{1+2(\gamma-1)M_1^2\frac{\cos^2\lambda_1}{\cos^2\lambda_2}\frac{\left[1+\frac{(\gamma-1)}{2}M_1^2\right]}{\left(\frac{p_2}{p_1}\right)^2}}-1\right] \tag{21}$$

also

$$\frac{u_2}{u_1}=\frac{u_2}{v_2}\frac{v_2}{v_1}\frac{v_1}{u_1}=\frac{\tan\lambda_2}{\tan\lambda_1}\frac{v_2}{v_1} \tag{22}$$

The expressions (3) and (4) for the blade forces may be written in nondimensional form as

$$\frac{Y}{sp_1}=1-\frac{p_2}{p_1}-\gamma M_1^2\cos^2\lambda_1\left(\frac{v_2}{v_1}-1\right) \tag{23}$$

$$\frac{X}{sp_1}=\gamma M_1^2\cos^2\lambda_1\left(1-\frac{\tan\lambda_2}{\tan\lambda_1}\frac{v_2}{v_1}\right) \tag{24}$$

As examples of the use of the preceding equations, losses and blade forces for a pressure-rise and a pressure-drop cascade have been computed and the results are listed in table I. For both cases an inlet Mach number of unity was assumed with inflow and outflow angles of 55° and 45°, respectively.

These flow angles, though possible for pressure rise, are impossible for pressure drop by incompressible-flow theory (under the condition of constant axial-flow area assumed here). The ideal quantities were first calculated and then for the loss case, new pressure ratios were assumed, which yielded the stagnation-pressure losses shown. It will be noted that the static-pressure ratio of 0.5, which yields a stagnation-pressure ratio of 0.942 in the pressure-drop case, is greater than the ideal static-pressure ratio. In incompressible flow it would have to be lower.

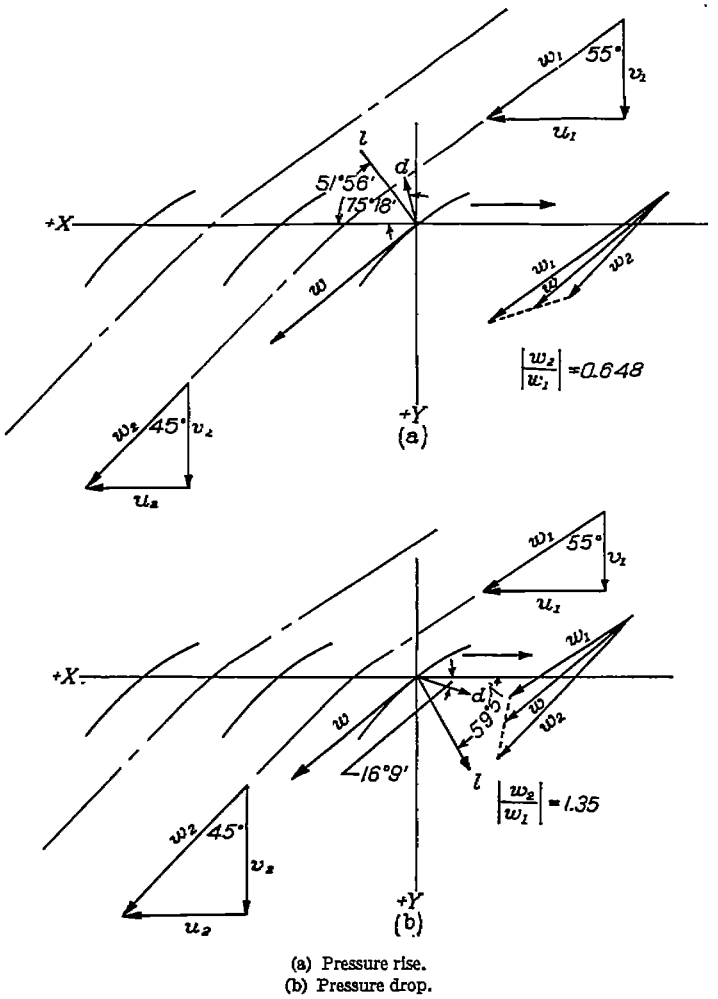

(a) Pressure rise.
(b) Pressure drop.

FIGURE 6.—Typical cascade forces and velocities.

The cascade-flow angles and forces are illustrated in figure 6. The resultant force l, the difference force d, and the mean velocity w bear no simple directional relation to each other. Because, in incompressible flow (under the conditions of constant axial-flow area assumed here), $v_2/v_1=1$ and, in high-solidity cascades, u_2/u_1 remains unchanged from the ideal case by equation (22), it is evident from equations (3) and (4) that only the static pressure can change in going from the ideal to the loss case. The incompressible difference force must therefore be in the axial direction. This conclusion for the incompressible case was reached in reference 1 by another method. The losses in high-speed cascade flow must evidently be considerably influenced by compressibility effects.

CONCLUSIONS

1. For inlet Mach numbers less than 0.4 in the normal operating range of an axial-flow pressure-rise stage, the relations for compressible and incompressible flow yield very nearly the same results. For larger inlet Mach numbers the discrepancies become considerable.

2. The compressible equations show the existence of nonideal operating ranges, which are not indicated by the incompressible equations. Conversely, certain operating ranges, which are excluded by the incompressible equations, are possible according to the compressible equations.

3. In certain ranges of the flow angles, two possible pressure ratios are predicted for given inlet Mach numbers and flow angles.

AIRCRAFT ENGINE RESEARCH LABORATORY,
NATIONAL ADVISORY COMMITTEE FOR AERONAUTICS,
CLEVELAND, OHIO, *August 1, 1945.*

REFERENCE

1. Mutterperl, William: High-Altitude Cooling. VI—Axial-Flow Fans and Cooling Power. NACA ARR No. L4I1le, 1944.

TABLE I-LOSSES AND BLADE FORCES FOR CASCADES IN COMPRESSIBLE FLOW

$[\lambda_1=55°;\ \lambda_2=45°;\ M_1=1]$

	Pressure rise		Pressure drop	
	Ideal	With losses	Ideal	With losses
Pressure ratio, p_2/p_1	1.522	[a] 1.4	0.461	[a] 0.5
Stagnation pressure ratio, $p_{s,2}/p_{s,1}$	1	0.950	1	0.942
Tangential force, $X/s\ p_1$	0.315	0.290	−0.143	−0.111
Normal force, $Y/s\ p_1$	−0.403	−0.307	0.199	0.192
Ratio of resultant force to difference force	∞	5.17	∞	7.66

[a] Assumed values.